Chemical Engineering Journal 316 (2017) 33–40

Contents lists available at ScienceDirect

Chemical Engineering Journal

journal homepage: www.elsevier.com/locate/cej

Adsorption mechanism of phosphate by polyaniline/TiO_2 composite from wastewater

Ning Wang, Jiangtao Feng, Jie Chen, Jianan Wang, Wei Yan *

Department of Environmental Science and Engineering, State Key Laboratory of Multiphase Flow in Power Engineering, Xi'an Jiaotong University, Xi'an 710049, PR China

HIGHLIGHTS

- The synergistic effect of the polyaniline and TiO_2 for the phosphate adsorption was investigated.
- Two efficient adsorption mechanisms were proposed.
- The ion exchange of phosphate with the chloride ion was verified.
- The binding force of Ti-P was the main pathway for the removal of phosphate.
- Polyaniline chains facilitate the regeneration of the composite adsorbent.

GRAPHICAL ABSTRACT

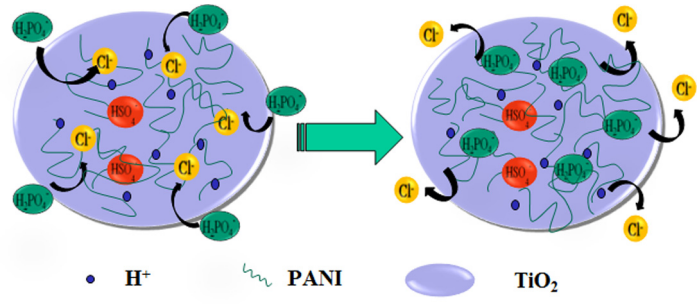

ARTICLE INFO

Article history:
Received 1 December 2016
Received in revised form 16 January 2017
Accepted 17 January 2017
Available online 19 January 2017

Keywords:
Desorption
Concentration
Kinetics
Isotherms
Synergistic effect

ABSTRACT

The adsorption behavior of polyaniline/TiO_2 (PANI/TiO_2) for phosphate from wastewater was investigated, and the mechanism was interpreted in details in this study. PANI/TiO_2 exhibited enhanced adsorption efficiency and high stability for phosphate removal in wide pH range (1–6) compared with PANI and TiO_2. The equilibrium time was much shorter than other similar sorbents reported, like HFO-201 and La-201, and 60 min was enough for the adsorption of 98% phosphate (10 mg P/L). After 5 times reuse of the NaOH (0.5 mol L^{-1}) for desorption, phosphate solution was concentrated from 10 mg P/L to 180 mg P/L without obvious loss of adsorption and desorption efficiency. The mechanism of the phosphate adsorption onto PANI/TiO_2 was revealed with the aid of SEM, XRD, EDS, FTIR and XPS. Two adsorption sites of protonated imino groups in PANI chains and the $Ti(OH)_n^{(4-n)+}$ from TiO_2 part were verified, and the binding force of Ti-P was the main pathway for the removal of phosphate. Generally, electrostatic interaction, ion-exchange and hydrogen bond were demonstrated to be involved during the adsorption. The synergistic effect of the PANI and TiO_2 make the organic/inorganic composite a promising sorbent for phosphate removal from wastewater.

1. Introduction

Phosphorus, as one of the indispensable elements and essential nutrients for human and other organisms is non-renewable and depletable [1]. However, the enrichment of phosphate in the water body would cause eutrophication and deterioration due to its inevitable use in agriculture industry [2]. The discharge concentration standard of the total phosphorus is getting more and more stringent, for instance, 0.5 mg P/L in China (GB 18918-2002) and 50 μg P/L in America (1994) [1]. Thus the removal of phosphate from water is faced with tremendous challenges. Although various methods, including chemical precipitation [3], crystallization [4] and biological enrichment [5], were employed in the past decades,

* Corresponding author.
E-mail address: yanwei@mail.xjtu.edu.cn (W. Yan).

http://dx.doi.org/10.1016/j.cej.2017.01.066
1385-8947/

they are reported either costly or effect-unsatisfactory [6], which can scarcely conform to the lower concentration discharge target .

Adsorption receives extensive attentions in recent years, due to its low-cost and high-efficient features, as well as easy-recycle of phosphate from dilute solution [7]. Among various adsorbents, like alum sludge [8], metal oxides [9–11], hydrated ferric oxides [12], periphyton [13], etc., the composites of organic polymer and inorganic metal oxide were frequently reported as adsorbents for phosphate removal in recent decades [14–16]. The superior adsorption performance of the composites is attributed to the advantages inherited from their parent materials [17]. PANI and TiO_2 were both reported as sorbents for the adsorption of anionic dyes [18,19], cationic dyes [20,21] and metal ions [22,23]. Wang et al. found PANI exhibited high adsorption capacity for Hg(II) (about 600 mg/g) at pH 4–6, and the imine, protonated imine and amine in the polymer matrix were verified to be the main sites for the mercury adsorption [24]. Asuha et al. found that the maximum adsorption capacities of the mesoporous TiO_2 for methyl orange (MO) and Cr(VI) are 454.5 and 33.9 mg/g [25]. However, the research of PANI/TiO_2 on the adsorption of pollutants from wastewater was seldom reported. Cheng et al. synthesized polyaniline-TiO_2 composite nanotubes for the removal of orange II and methyl orange, and the mechanism was interpreted to be mainly photodegradation [26]. Given these findings, it inspired us to exploit the synergistic effect of PANI and TiO_2 for the adsorption of anions like phosphate.

In this study, the PANI/TiO_2 composite was fabricated for phosphate removal from contaminated water. It was found that PANI/TiO_2 possessed high adsorption efficiency for phosphate in wide pH range (1–6) and can be readily regenerated by low concentration NaOH (0.5 mol L^{-1}) solution. The effects of pH, temperature, dosage, as well as the competing anions on the adsorption of phosphate were studied; the kinetics and isotherms of the adsorption process were also investigated by fitting the experimental data with typical kinetics and isotherms models. The application of the novel sorbent in actual municipal wastewater and the concentration of phosphate by adsorption-desorption recycles were both carried out to test the practicability in industry. Moreover, the structural changes on the polyaniline and TiO_2 during adsorption process were demonstrated to propose the adsorption-desorption mechanisms of the phosphate by PANI/TiO_2.

2. Materials and methods

2.1. Materials

Aniline (99.5%, Sinopharm Chemical Reagent Co., Ltd, Shanghai, China) was distilled under reduced pressure twice, and then stored in dark at 0 °C in N_2 atmosphere before used. Analytical grade reagents of ammonium persulphate (APS), HNO_3, HCl, KH_2PO_4, NaCl, NaOH, Na_2SO_4, $NaNO_3$ purchased from Sinopharm Chemical Reagent Co., Ltd. (Shanghai, China) were used as received. The actual municipal effluent was derived from a municipal wastewater treatment plant in Xi'an (China). The working solutions of different phosphate concentrations were prepared by diluting the stock KH_2PO_4 solutions (1000 mg P/L). The deionized water used for all the experiments was prepared by an EPED-40TF Superpure Water System (EPED, China).

2.2. Preparation of PANI/TiO_2

PANI/TiO_2 was formed by the chemical oxidative polymerization of aniline monomer in the TiO_2 solution prepared by the sol-gel hydrolysis according to the literature [27]. The typical process is as follows: the dispersed TiO_2 sol in 100 mL HNO_3 (0.1 mol L^{-1}) was magnetically stirred for 1.0 h. Then, aniline (1.8 mL) monomer was added and stirred for 1 h. APS solution (0.1 mol L^{-1}) was added and reacted for 8 h at ambient temperature. Finally, the composite was filtrated and washed with a large amount of deionized water and dried at 50 °C for 48 h. For comparison, the PANI, TiO_2 was also prepared followed the process as above.

2.3. Sample characterization

Samples were washed for several times by deionized water and dried at 50 °C for 48 h before all characterizations maintained below. The morphology of the composites at different stages was characterized by scanning electron microscopy (SEM, JSM-6700F, Japan; JJSM-6390A, JEOL instrument), and the energy dispersive X-ray spectrometry (EDS) was used to determine elements of the adsorbents. The Brunauer-Emmett-Teller specific surface area (S_{BET}), total pore volume (V), and average pore radius (R) were determined by the Builder SSA-4200 (Beijing, China) at 77K using the Barrett-Joyner-Halenda (BJH) method. X-ray Diffraction (XRD) were analyzed by an X'Pert PRO MRD Diffractometer using Cu-Kα radiation (λ = 1.5418 Å). The X-ray photoelectron spectroscopy (XPS) was performed on Kratos Axis Ultra DLD with an Al monochromatic X-ray source (1486.71 eV), and all binding energies (BEs) were referenced to the C1 s hydrocarbon peak at 284.8 eV. FT-IR spectra of samples were measured using the KBr pellet method on a BRUKER TENSOR 37 FT-IR spectrophotometer in the range of 4000–400 cm^{-1}.The zeta potentials of adsorbents were measured with Malvern Zetasizer Nano ZS90, through adding 5 mg sample in 10 mL NaCl solution (10^{-3} mol L^{-1}) at different pH values (adjusted with diluted HNO_3 or NaOH solution).

2.4. Adsorption and desorption studies

All the batch adsorption experiments were conducted on a temperature controlled shaker at 200 rpm in dark. Then the suspension was centrifuged. Phosphate concentration was determined photometrically with the molybdenum blue method [28]. NaOH (0.1 mol L^{-1}) and HCl (0.1 mol L^{-1}) were used as elution and activation agents. In the adsorption kinetics experiment, the suspension was sampled at regular intervals, and filtrated immediately with Syringe-driven Filter (0.45 μm). In order to study the effect of competing anions (SO_4^{2-}, NO_3^- and Cl^-) (in the sodium salt form), the phosphate adsorptions were measured in presence of these three ions. NaOH solution was used for the phosphate stripping. The adsorption rate (R), adsorption capacity (q_t), desorption capacity (q_{de}) and efficiency (R_{de}) based on the corresponding adsorption rate and capacity were calculated by Eqs. (1)–(6) in Appendix S1, respectively.

The phosphate enrichment was implemented by reutilizing the stripping solution (0.5 mol L^{-1} NaOH was used) for five cycles with 0.125 L stripping solution per g adsorbent. Both of the adsorption and desorption were equilibrated for 24 h at 25 °C at an oscillator with 220 rpm.

3. Results and discussion

3.1. Morphological and structural properties

The morphologies of composite were composed of uniform granules with 1 μm of average diameter according to the SEM image in Fig. 1a. The pretreatment by NaOH-HCl and adsorption of phosphate did not change the morphology of the composite (see Fig. S1). The textural properties of samples are listed in Table 1. No significant change occurred in the S_{BET} (m^2 g^{-1}), V (cm^3 g^{-1}), and R (nm) of three samples during the treatment and the

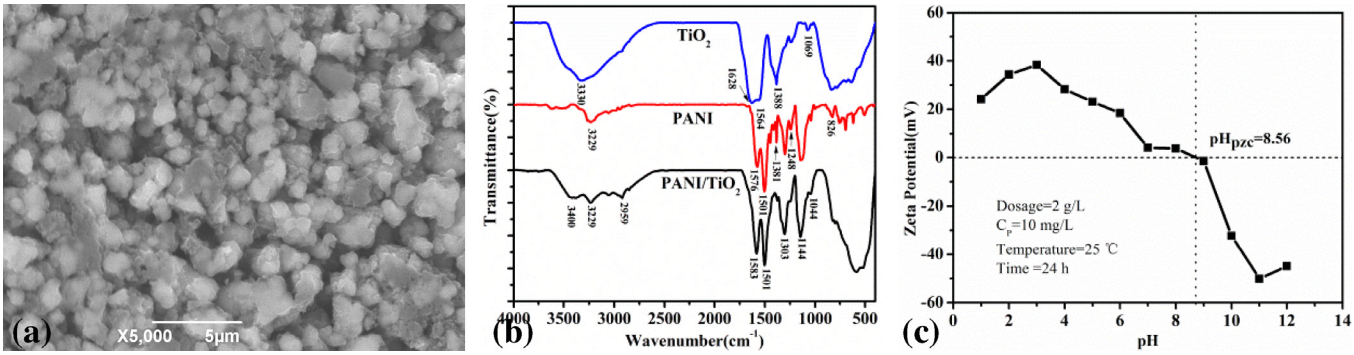

Fig. 1. Characterizations of PANI/TiO_2: (a)SEM images, (b)FTIR spectra, (c) Zeta potential as a function of pH.

Table 1
Textural properties of the different samples.

Samples (PANI/TiO_2)	S_{BET}($m^2\ g^{-1}$)	V($cm^3\ g^{-1}$)	R(nm)
Before pretreatment	11.60	0.04378	755
NaOH-HCl treated	11.81	0.03797	643
After adsorption	12.56	0.03706	590

adsorption. It was indicated that there was no obvious relationship between the morphology, textural properties and the adsorption.

In the FTIR spectrum of PANI/TiO_2, the characteristic peaks of both PANI and TiO_2 were all observed by comparing with the spectra of PANI and TiO_2 in Fig. 1b. The broad peak at 500–700 cm^{-1} corresponded to the Ti-O-Ti bending mode. For PANI, the characteristic peaks of benzenoid units located at 1501, 1381, 1303, 1248, 826 and 801 cm^{-1}, and quinoid units at 1576, 1340 and 1144 cm^{-1} [29]. The peak at 1144 cm^{-1} was attributed to the doping imine in the PANI chain, implying the synthesized PANI in PANI/TiO_2 was the emeraldine salt (PANI-ES) [30]. The peak at 1576 cm^{-1} in the PANI spectrum shifted to 1583 cm^{-1} and the hydroxyl wide peak at 3330 cm^{-1} on TiO_2 also changed in the spectrum of PANI/TiO_2 indicating the chemical reactions occurred during the composition. The EDS (Fig. S2a) also confirmed the composite of TiO_2 and PANI. No characteristic peak of the doped PANI was observed in the XRD pattern of PANI/TiO_2 (Fig. S3), which was reported to be amorphous [31]. The crystalline of TiO_2 in the synthesized composite was mainly anatase.

The properties of surface potential at different pH plays a significant role for an adsorbent in terms of electrostatic interactions between the adsorbent and adsorbate [32]. From Fig. 1c, it can be seen that the potential of TiO_2/PAN decreased with the pH and pH_{ZPC} of the composite was about 8.56. When the solution pH is above 8.56, the composite is negatively charged, resulting in anion repulsion between sorbents and phosphate; when pH was below 8.56, electrostatic attraction of the phosphate ion on the adsorbent occurred due to the positive charge on the composite.

3.2. Adsorption studies

All the adsorption experiments were performed with the sorbents dosage of 2 g L^{-1}, which was determined by varying the dosage of the PANI/TiO_2 (Fig. S4).

Environment pH during adsorption is of importance, which can influence not only phosphate species but also the surface properties of sorbents [16]. According to Fig. 2, the optimal pH for adsorption was below 6. When the pH increased above 6, the P removal rate decreased significantly, due to the competing of the hydroxyl group on the sorbent in alkaline condition and the anion repulsion between sorbents and phosphate according to the Zeta potential

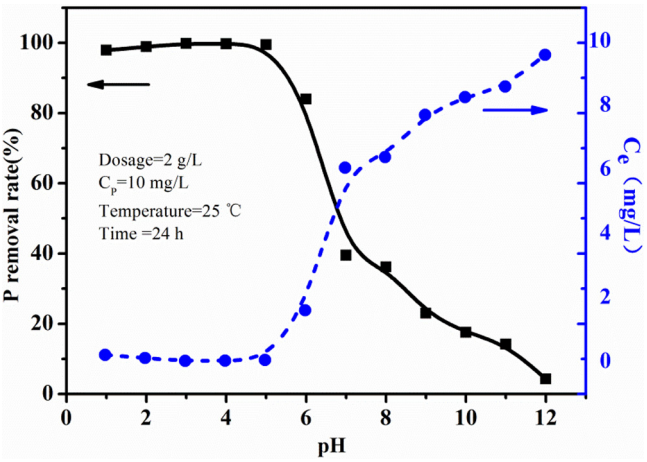

Fig. 2. Effect of pH on adsorption efficiency.

study. This phenomenon was regarded as a strong confirmation for the existence of electrostatic interaction. Fig. S5 showed that the pH during the adsorption for 24 h stabilized at about 3, at which the main form of phosphate was $H_2PO_4^-$ (Fig. S6) [2], revealing that $H_2PO_4^-$ was the main form when the adsorption occurred.

In addition, according to Figs. 1c and 2, when the surface potential of the PANI/TiO_2 was negatively less than −30 mV at pH 11, there was still 18% of P adsorption, which indicated that there is not only electrostatic attraction, but also other interactions involving in this part of adsorption.

The adsorption efficiency against time at different temperatures was determined to investigate the adsorption kinetics. The adsorption equilibrium of phosphate on PANI/TiO_2 could be achieved in 60 min for the selected temperatures with more than 98% of adsorption efficiency. In order to investigate the adsorption rate-controlling mechanism of phosphate adsorption process, the data were analyzed by the Pseudo-first-order, Pseudo-second-order, Elovich mass transfer and Power function kinetic models [33–35], respectively. The data plots and fitted curves are depicted in Fig. 3a, b, and c with the corresponding expression formulas and parameters listed in Table S1.

Evidently, the adsorption process fitted well with the Pseudo-second-order model for the highest correlation coefficients (R^2) and lower S.D. value (calculated by Eq. (7) in Appendix S2) compared with other models, which was in accord with most of sorbents reported [36,37]. It was indicated that the adsorption process of phosphate onto PANI/TiO_2 was mainly monolayer and chemical adsorption [21,38].

Choi et al. [33] found that temperature has positive effect on the phosphate adsorption capacity onto the synthesized MIO

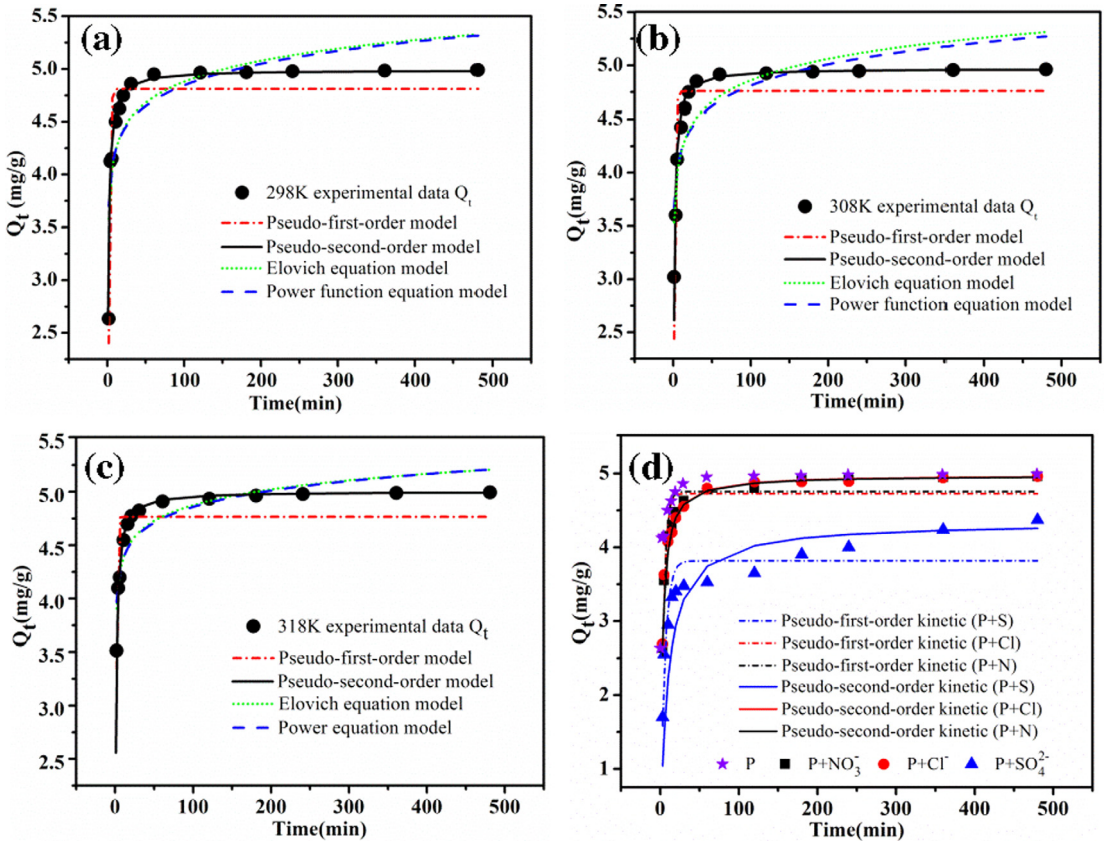

Fig. 3. Adsorption kinetics plots at 298 K (a), 308 K (b), 318 K (c) and 298 K with anions (d).

magnetite, which was attributed to that the phosphate was not physically but chemically adsorbed onto the MIO. The endothermic nature of the phosphate adsorption was also reported by many researchers [39,40]. Interestingly, opposite conclusion was also reported for phosphate adsorption by Zheng et al. [41], who found a slight decrease in the phosphate uptake by mesoporous hybrid film with the temperature increasing. According to the Fig. S7 and Table S1, the effect of temperature on phosphate adsorption was faint, and the initial adsorption rate ($h = k_2 q_e^2$) were temperature independent. According to the temperature effect and the kinetics study, it might be concluded that the adsorption of phosphate onto PANI/TiO_2 was both physical absorption and chemisorption, and chemisorption was the rate-controlling step.

The isotherm studies with various initial concentrations were carried out at 298 K for 24 h. The experimental data are manifested in Fig. 4a, where the equilibrium adsorption capacity was improved with the increasing of initial phosphate concentration. Oppositely, the phosphate removal rate decreased. Four isotherm models, the Langmuir, Freundlich, Temkin and D-R isotherm models, were employed to investigate the interaction between phosphate and PANI/TiO_2 composite (Fig. 4b and c).

According to the value of R^2 and S.D. of each model (Table S2 and Fig. 4c), the applicability of the above three models for the adsorption of phosphate onto PANI/TiO_2 followed the order as: Langmuir > Temkin > Freundlich > D-R. The experimental data can be fitted to Langmuir isotherm model best. The maximum phosphate adsorption capacity of PANI/TiO_2 was calculated to be 12.11 mg g^{-1}.

It was reported that binding energy involving in physisorption process was in the range of 1–8 kJ mol^{-1}, corresponding to the parameter b (1.81 kJ mol^{-1}) from Temkin isotherm model [42,43]. As for the D-R isotherm model, the mean free energy of

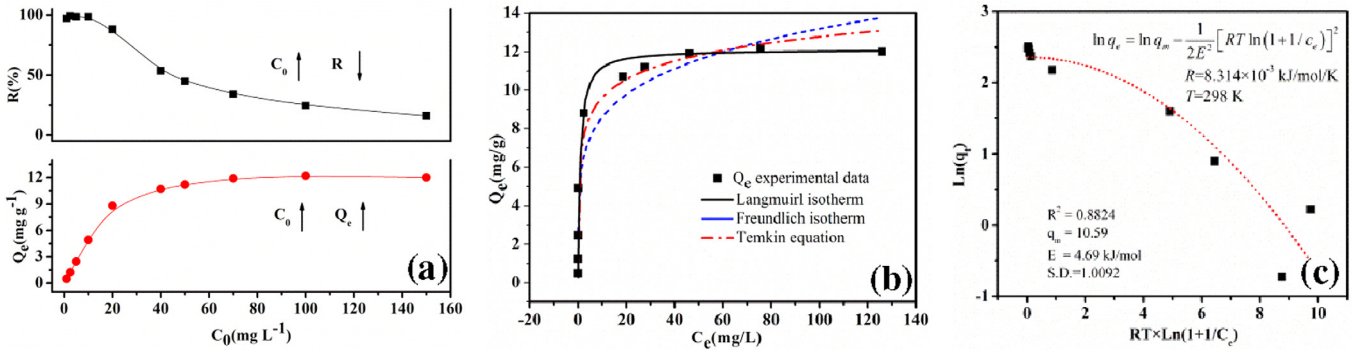

Fig. 4. The isotherm studies (a) experimental data; (b) the isotherm models plot; (c) the D-R model plot and corresponding parameters.

adsorption (E) was adopted to determine the adsorption mechanisms. The range of 8 and 16 kJ mol^{-1} was assigned to be ion-exchange in the adsorption process, less than 8 kJ mol^{-1} to be physisorption [13]. The E value was 4.69 kJ mol^{-1} close to 8 kJ mol^{-1}, showing that the adsorption process was physical in nature and ion-exchange interaction might involve.

Three common anions, including SO_4^{2-}, NO_3^-, and Cl^-, were employed to investigate the effect of the coexisting anions and the ionic strength on the phosphate adsorption onto PANI/TiO_2. The effect of NO_3^- and Cl^- was very slight, and the present of SO_4^{2-} can impact phosphate adsorption significantly, even though the concentration was very low (Fig. S8). In order to study the ionic strength effect on adsorption, the concentration of Cl^- (NaCl) was expanded. The trend of P adsorption capacity (Fig. S8) implied that the ionic strength would influence the adsorption, indicating the existence of electrostatic interaction during adsorption process [44].

In addition, the adsorption kinetic study in the presence of SO_4^{2-}, NO_3^-, and Cl^- was also achieved. The experimental data was fitted with Pesudo-first-order and Pesudo-second order models (Fig. 3d and Table S3). It can be concluded from the results that the influence of three anions on the adsorption followed the order of $SO_4^{2-} > NO_3^- > Cl^-$ by comparing k_1, k_2 and the initial adsorption rate ($k_2 q_e^2$), and the existences of these anions would not change the adsorption mechanism. The chemisorption mechanism was still the rate-controlling step. The remarkable influence of SO_4^{2-} was observed in most sorbents reported, and two mechanisms were promoted: rising the solution pH [45] and the ligand exchange with phosphate [46,47]. As the pH in this study during the adsorption was stable at about 3 (Fig. S5), the competing adsorption through ligand exchange with phosphate was assumed to be the major influencing mechanism by SO_4^{2-}.

3.3. Desorption studies

Desorption efficiency is an important factor in evaluating the utilizability of the sorbents. According to the Figs. 1c and 2, alkaline environment in solution was favor for desorption of the adsorbed phosphate from PANI/TiO_2. Fig. 5a depicted desorption efficiencies by NaOH with different concentrations and the corresponding re-adsorption efficiencies. The desorption efficiency increased slightly with the concentration of NaOH increasing and the maximum desorption efficiency was 95% by 2 mol L^{-1} NaOH. However, this group showed unexpectedly poor re-adsorption performance, which was assumed that higher concentration of NaOH would exhibit irreversible impact on the sorbents.

Desorption kinetics was investigated by 0.5 mol L^{-1} NaOH (Fig. S9). It was indicated that in the first 60 min the desorption rate increased rapidly and reached above 85%. Then the data point rose slowly and finally reached above 98% after 8 h.

The reusability of the composite sorbent for imitated wastewater (10 mg P L^{-1}) and actual municipal wastewater (53 mg P L^{-1}) was both assessed, and the results are illustrated in Fig. 5b. The adsorption efficiency maintained above 96% for imitated wastewater and 50% for actual wastewater after eight cycles of phosphate adsorption-desorption, indicating the sorbent in this study was relatively stable for engineering application.

In this study, the stripping solution was reused to enrich the phosphate for further recovery, which could also lowered the desorption cost (Fig. S10 and Table S4). It was found that the regenerated sorbent also exhibit 98% of phosphate removal rate after 5 cycles, indicating the reuse of the NaOH solution would not decrease the adsorption efficiency. The phosphorus was concentrated from 10 mg/L to 180 mg/L, revealing the enrichment of the phosphate by PANI/TiO_2 was feasible and efficient.

By comparing PANI/TiO_2 with other composite sorbents on phosphate adsorption (Table S5), it can be found that PANI/TiO_2 outstood for wide pH range, quick equilibrium and excellent regeneration ability, indicating PANI/TiO_2 as a potential sorbent for phosphate (Appendix S4). Therefore, it is necessary to uncover the adsorption-desorption mechanisms in the process.

3.4. Adsorption-desorption mechanisms

FTIR spectra of PANI/TiO_2 before and after adsorption were analyzed to determine the changes of functional groups (Fig. S11). No significant change happened during the treatment and adsorption process. The assignments of characteristic peaks are listed in Table S6. Notably, the peak at 1144 cm^{-1} was associated with high electron delocalization in PANI, which was assumed as the doping form of the PANI [30]. This peak disappeared after NaOH treatment, and appeared again in the following HCl treatment and phosphate adsorption, corresponding to the presence of hydrogen sulfate or chlorine counter-ions [48]. In addition, the doping of SO_4^{2-} (from APS when synthesis) and NO_3^- was verified at 1044 cm^{-1} [49] and 1388 cm^{-1} [50]. It was indicated that during the pretreatment and adsorption, there occurred deprotonation and protonation.

According to the EDS analysis (Fig. S2 and Table S7), when the synthesized PANI/TiO_2 was pretreated by NaOH, the sulfur weight content decreased significantly, so as the oxygen weight content, implying the de-doping of SO_4^{2-} on the PANI chains. The chlorine

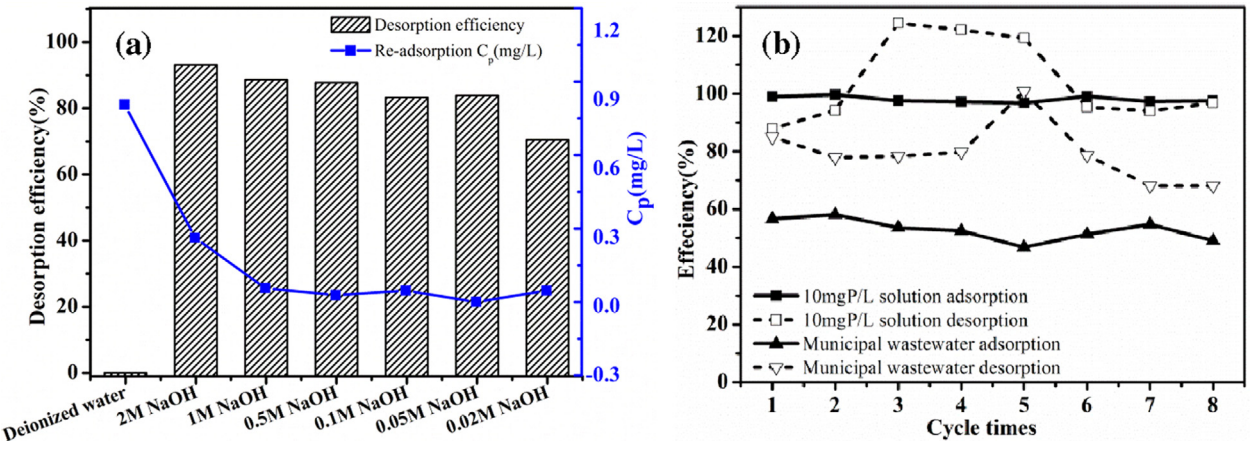

Fig. 5. The desorption and re-adsorption studies on PANI/TiO_2, (a) Effect of NaOH concentration, (b) adsorption-desorption cycles in wastewater samples.

presented after HCl pretreated, indicating the doping of protonic acid. After adsorption, the phosphorus was detected with the decrease of the chlorine. The amount of chlorine ion after adsorption was determined by silver mirror reaction in Mohr method (see Appendix S2). The adsorption of phosphate caused 0.52 mmol L^{-1} of chlorine ions increasing compared with the control group (Table S8), indicating the ion-exchange of phosphate and chlorine ion. Theoretically, the maximum release amount of chlorine ion by ion-exchange reaction should be equal to the amount of phosphate in solution (C_p = 0.32 mmol L^{-1}), the extra release of chlorine anions would be deliberated later.

The adsorption efficiencies by PANI and TiO_2 (Table S8) showed that TiO_2 played predominant role in the phosphate adsorption (89.1%) and the adsorption of phosphate by PANI was only 10.68%, which was much different with the result of ARG adsorption by PANI/TiO_2 reported before [50], indicating that the involving mechanisms differed greatly.

In addition, further study by XPS characterization was fulfilled. The B.E. of S $2p_{3/2}$ component at about 168.0 eV before adsorption, and Cl $2p_{3/2}$ at 197.6 eV after adsorption were detected in Fig. S12. The P2p component was also detected at about B.E. of 133.14 eV. Zhang [51] reported that the binding energy of phosphate captured by amine structure from D-201 was observed at 131.9 eV, while the La–P interaction had a higher binding energy. Therefore, the binding energy at 133.14 eV was attributed to the higher interaction of Ti and P in this study. On the basis the higher contribution of TiO_2 in the phosphate adsorption (Table S8), the Ti–P interaction may be the main mechanism. The properly curve-fitted N 1s core-level spectrums of PANI/TiO_2 before and after adsorption are shown in Fig. 6a and b. The two major peaks at B.E. of 399.3 ± 1 eV and 398.1 ± 1 eV are assigned to the amine (–NH–) and imine (=N–) structures, respectively [29,30]. Also, a small signal peak can be observed at >400 eV, attributed to the positively charged nitrogen (N^+) [30]. No significant change was observed from Fig. 6a and b, indicating that the adsorption of phosphate would not affect the structure of the PANI chains.

Taking account into the analyses above, the adsorption process on TiO_2 parts in the synthesized sorbents can be deduced as follows in Fig. 7.

According to Figs. S3 and 1b, TiO_2 part synthesized in this study was mainly hydrated titanium oxide for the lack of calcining. Sugimoto et al. reported that hydrated titanium oxide, expressed as $Ti(OH)_n^{(4-n)+}$, had three complex species including $Ti(OH)_2^{2+}$, $Ti(OH)_3^+$ and $Ti(OH)_4$ in different pH range [52]. When the hydrated titanium oxide was treated by NaOH, the main species of microemulsions was $Ti(OH)_4$ ((a) in Fig 7). Then it transferred to be $Ti(OH)_2^{2+}$ and $Ti(OH)_3^+$ mixtures ((b) in Fig 7) with chlorine anions adsorbed by electrostatic interaction when treated by HCl. The chlorine anions in TiO_2 before and after adsorption were verified by EDS analyses (Fig. S13 and Table S9). During the adsorption of phosphate, the original phosphate solution with pH of about 6 increased the pH of adsorption solution, the $Ti(OH)_2^{2+}$ species were transformed into $Ti(OH)_3^+$, and corresponding chlorine anions fled from the structure, which accounted for the extra chlorine released

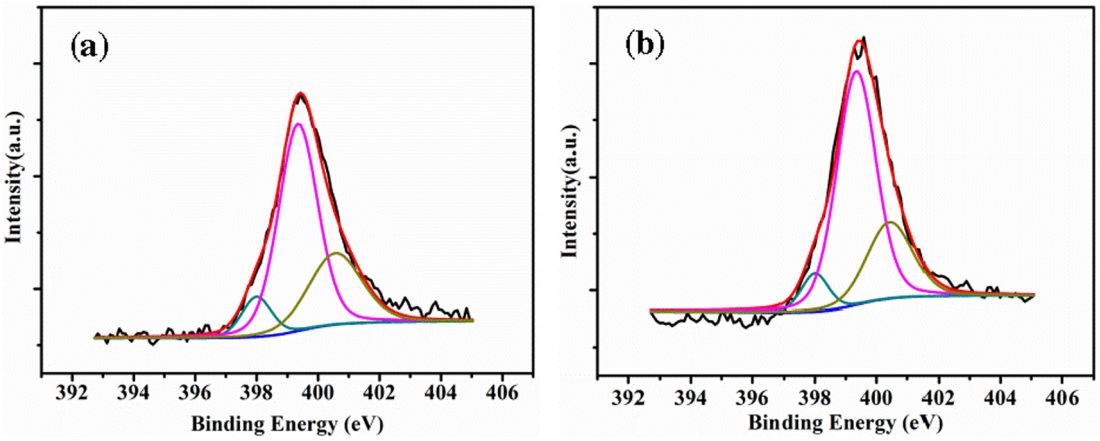

Fig. 6. The curve-fitted N 1s core-level spectrums of PANI/TiO_2 before (a) and after (b) adsorption.

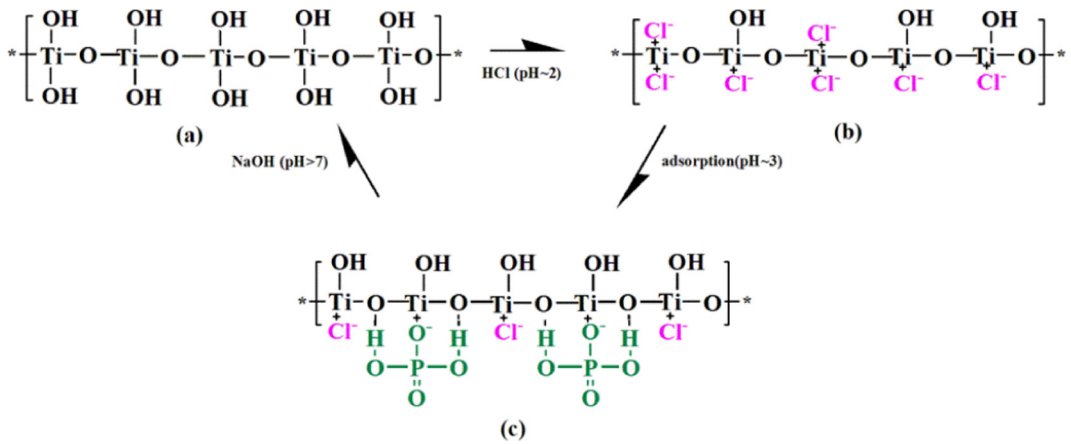

Fig. 7. The phosphate adsorption process happened on synthesized TiO_2.

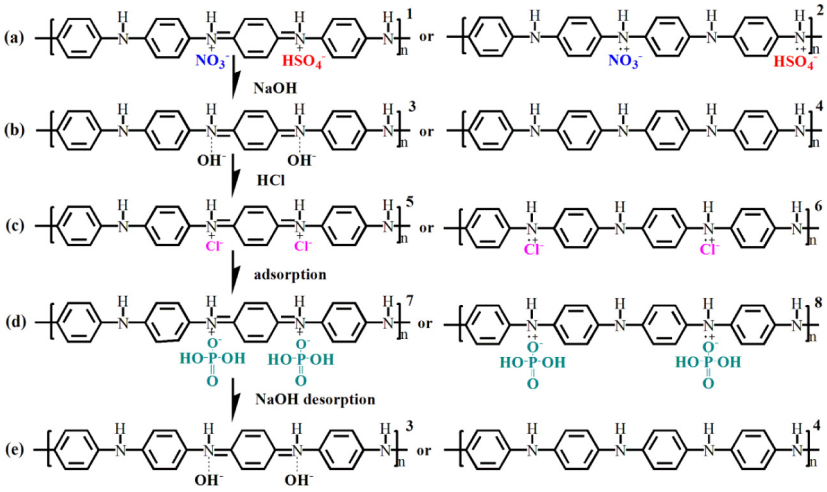

Fig. 8. The proposed doping and ion-exchange during adsorption process.

from sorbent after adsorption. Sugimoto et al. [53] also reported that the increase of pH would enhanced the adsorption of OH^- on $Ti(OH)_4$, thus causing the micro-emulsions charged negatively, resulting in the desorption of phosphate, and the closed ring of recycle was formed.

To conclude the above analysis, the electrostatic interaction, ion-exchange, and hydrogen-bond, as well as Ti–P interaction involved in the adsorption of phosphate on the part of TiO_2.

Although the contribution of PANI on the adsorption of phosphate was puny (Table S8), the reversible redox properties of PANI were significant in the regeneration of the sorbent [54]. The adsorption process of phosphate involving protonation, deprotonation and ion-exchange reaction was deduced in Fig. 8. Herein, eight characteristic species of PANI chains are used to demonstrate the adsorption process happened on PANI part.

(a) The synthesized PANI chains were PANI-ES state, doping with NO_3^- and HSO_4^- (Fig. S11 and Table S6);
(b) When eluted by NaOH, the PANI-ES were transformed into PANI-EB state by de-doping;
(c) Protonic acid doping by HCl introduced chlorine anions into PANI chains as the counter anions (Fig. S14 and Table S10);
(d) Ion-exchange of phosphate and chlorine ions occurred during adsorption, confirmed by EDS;
(e) The exhausted adsorbent was treated by NaOH (0.1 mol L^{-1}), excess OH^- may make the PANI-EB negatively charged, and desorption was achieved.

Combining the analyses of phosphate adsorption on TiO_2 and PANI, the adsorption mechanism of PANI/TiO_2 was suggested and sketched in Fig. S15.

4. Conclusion

PANI/TiO_2 synthesized in this study was a promising adsorbent for phosphate removal. The encouraging properties as sorbent for phosphate contained the wide pH range of application (1–6), rapid adsorption equilibrium (60 min), and easy desorption-regeneration (maintained 95% adsorption efficiency after 8 cycles), and also low-cost desorption and concentration (from 10 to 180 mg g^{-1} by 5 mL of 0.5 mol L^{-1} NaOH). The faint effect of temperature revealing both physical absorption and chemisorption occurred during the adsorption process. The adsorption mechanism was interpreted to be the collaboration of electrostatic attraction, hydrogen-bond interaction, and ion exchange reactions by FTIR, EDS and XPS. And the main site for adsorption of phosphate was attributed to TiO_2 part, which is different with previous study for dye adsorption.

Given reports on the adsorption capacity by PANI and TiO_2 for cationic and anionic dyes, as well as metal anion, the superiority of PANI/TiO_2 as a perspective sorbent, should be fully developed, and co-adsorption of pollutants should be the next focus to maximize its potential.

Acknowledgments

This work was gratefully supported by the National Natural Science Foundation of China [grant number 21307098]; the National Natural Science Foundation of China [grant number 21507104].

Appendix A. Supplementary data

Supplementary data associated with this article can be found, in the online version, at http://dx.doi.org/10.1016/j.cej.2017.01.066.

References

[1] X. Liu, L. Zhang, Removal of phosphate anions using the modified chitosan beads: adsorption kinetic, isotherm and mechanism studies, Powder Technol. 277 (2015) 112–119.
[2] D. Zhao, J.P. Chen, Application of zirconium/PVA modified flat-sheet PVDF membrane for the removal of phosphate from aqueous solution, Ind. Eng. Chem. Res. 55 (2016) 6835–6844.
[3] Z. Zhen, D. Hu, W. Qiao, G. Chen, L. Jiang, Z. Li, S. Mai, Optimization for phosphorous removal in thickening and dewatering sludge water by polyaluminum chloride, Environ. Sci. (China) 35 (2014) 2249–2255.
[4] W. Li, L. Zeng, Y. Kang, Q. Zhang, J. Luo, X. Guo, A solid waste, crashed autoclaved aerated concrete, as a crystalline nucleus for the removal of low concentration of phosphate, Desalin. Water Treat. 57 (2015) 14169–14177.
[5] Y. Law, R.H. Kirkegaard, A.A. Cokro, X. Liu, K. Arumugam, C. Xie, M. Stokholm-Bjerregaard, D.I. Drautz-Moses, P.H. Nielsen, S. Wuertz, R.B. Williams, Integrative microbial community analysis reveals full-scale enhanced biological phosphorus removal under tropical conditions, Sci. Rep. 6 (2016) 25719–25734.
[6] B. Pan, J. Wu, B. Pan, L. Lv, W. Zhang, L. Xiao, X. Wang, X. Tao, S. Zheng, Development of polymer-based nanosized hydrated ferric oxides (HFOs) for enhanced phosphate removal from waste effluents, Water Res. 43 (2009) 4421–4429.
[7] J. Lalley, C. Han, X. Li, D.D. Dionysiou, M.N. Nadagouda, Phosphate adsorption using modified iron oxide-based sorbents in lake water: kinetics, equilibrium, and column tests, Chem. Eng. J. 284 (2016) 1386–1396.
[8] Y. Kuwahara, T. Ohmichi, T. Kamegawa, K. Mori, H. Yamashita, A novel conversion process for waste slag: synthesis of a hydrotalcite-like compound and zeolite from blast furnace slag and evaluation of adsorption capacities, J. Mater. Chem. 20 (2010) 5052–5062.

[9] P. Delaney, C. McManamon, J.P. Hanrahan, M.P. Copley, J.D. Holmes, M.A. Morris, Development of chemically engineered porous metal oxides for phosphate removal, J. Hazard. Mater. 185 (2011) 382–391.
[10] M. Li, J. Liu, Y. Xu, G. Qian, Phosphate adsorption on metal oxides and metal hydroxides: a comparative review, Environ. Rev. 24 (2016) 319–332.
[11] S. Moharami, M. Jalali, Effect of TiO_2, Al_2O_3, and Fe_3O_4 nanoparticles on phosphorus removal from aqueous solution, Environ. Prog. Sustainable Energy 33 (2014) 1209–1219.
[12] D. Conidi, W.J. Parker, The effect of solids residence time on phosphorus adsorption to hydrous ferric oxide floc, Water Res. 84 (2015) 323–332.
[13] H. Lu, L. Yang, S. Shabbir, Y. Wu, The adsorption process during inorganic phosphorus removal by cultured periphyton, Environ. Sci. Pollut. Res. Int. 21 (2014) 8782–8791.
[14] Y.G. Ko, T. Do, Y. Chun, C.H. Kim, U.S. Choi, J.Y. Kim, CeO_2-covered nanofiber for highly efficient removal of phosphorus from aqueous solution, J. Hazard. Mater. 307 (2016) 91–98.
[15] X. Ju, J. Hou, Y. Tang, Y. Sun, S. Zheng, Z. Xu, ZrO_2 nanoparticles confined in CMK-3 as highly effective sorbent for phosphate adsorption, Microporous Mesoporous Mater. 230 (2016) 188–195.
[16] Q. Zhang, Z. Zhang, J. Teng, H. Huang, Q. Peng, T. Jiao, L. Hou, B. Li, Highly efficient phosphate sequestration in aqueous solutions using nanomagnesium hydroxide modified polystyrene materials, Ind. Eng. Chem. Res. 54 (2015) 2940–2949.
[17] J. Chen, J. Feng, W. Yan, Influence of metal oxides on the adsorption characteristics of PPy/metal oxides for Methylene Blue, J. Colloid Interface Sci. 475 (2016) 26–35.
[18] A. Alshameri, C. Yan, X. Lei, Enhancement of phosphate removal from water by TiO_2/Yemeni natural zeolite: preparation, characterization and thermodynamic, Microporous Mesoporous Mater. 196 (2014) 145–157.
[19] P.A. Connor, A.J. McQuillan, Phosphate adsorption onto TiO_2 from aqueous solutions an in situ, Langmuir 15 (1999) 2916–2921.
[20] L.R. M. Grassi, V. Belgiorno, Organic contaminants removal from wastewater by adsorption on granular TiO_2 a study with methylene blue, Proceedings of the 11th International Conference on Environmental Science and TechnologyChania, Crete, Greece, 2009.
[21] M.M. Ayad, A. Abu, El-Nasr, Adsorption of cationic dye (methylene blue) from water using polyaniline nanotubes base, J. Phys. Chem. C 114 (2010) 14377–14383.
[22] B. Qiu, C. Xu, D. Sun, Q. Wang, H. Gu, X. Zhang, B.L. Weeks, J. Hopper, T.C. Ho, Z. Guo, S. Wei, Polyaniline coating with various substrates for hexavalent chromium removal, Appl. Surf. Sci. 334 (2015) 7–14.
[23] T.S. Najim, A.J. Salim, Polyaniline nanofibers and nanocomposites: preparation, characterization, and application for Cr(VI) and phosphate ions removal from aqueous solution, Arabian J. Chem. (2014).
[24] J. Wang, B. Deng, H. Chen, X. Wang, J. Zheng, Removal of aqueous Hg(II) by polyaniline: sorption characteristics and mechanisms, Environ. Sci. Technol. 43 (2009) 5223–5228.
[25] S. Asuha, X.G. Zhou, S. Zhao, Adsorption of methyl orange and Cr(VI) on mesoporous TiO_2 prepared by hydrothermal method, J. Hazard. Mater. 181 (2010) 204–210.
[26] Y. Cheng, L. An, F. Gao, G. Wang, X. Li, X. Chen, Simplified synthesis of polyaniline-TiO_2 composite nanotubes for removal of azo dyes in aqueous solution, Res. Chem. Intermed. 39 (2012) 3969–3979.
[27] C. Liu, L. Fu, J. Economy, A simple, template-free route for the synthesis of mesoporous titanium dioxide materials, J. Mater. Chem. 14 (2004) 1187–1189.
[28] J. Murphy, J.P. Riley, A modified single solution method for the determination, Anal. Chim. Acta 27 (1962) 31–39.
[29] E.T. Kang, K.G. Neoh, K.L. Tan, Polyaniline: a polymer with many interesting intrinsic redox states, Prog. Polym. Sci. 23 (1998) 277–324.
[30] E.T. Kang, K.G. Neoh, K.L. Tan, ESCA studies of protonation in PANI, Polym. J. 21 (1989) 873–881.
[31] K. Lee, S. Cho, S.H. Park, A.J. Heeger, C.W. Lee, S.H. Lee, Metallic transport in polyaniline, Nature 441 (2006) 65–68.
[32] F. Deng, L. Min, X. Luo, S. Wu, S. Luo, Visible-light photocatalytic degradation performances and thermal stability due to the synergetic effect of TiO_2 with conductive copolymers of polyaniline and polypyrrole, Nanoscale 5 (2013) 8703–8710.
[33] J. Choi, J. Chung, W. Lee, J.O. Kim, Phosphorous adsorption on synthesized magnetite in wastewater, J. Ind. Eng. Chem. 34 (2016) 198–203.
[34] L. Zeng, X. Li, J. Liu, Adsorptive removal of phosphate from aqueous solutions using iron oxide tailings, Water Res. 38 (2004) 1318–1326.
[35] G. McKay, Y.S. Ho, J.C.Y. Ng, Biosorption of copper from waste waters: a review, Sep. Purif. Rev. 28 (1999) 87–125.
[36] Y.S. Ho, Second-order kinetic model for the sorption of cadmium onto tree fern: a comparison of linear and non-linear methods, Water Res. 40 (2006) 119–125.
[37] Y.S. Ho, Review of second-order models for adsorption systems, J. Hazard. Mater. 136 (2006) 681–689.
[38] M.A. Salem, The role of polyaniline salts in the removal of direct blue 78 from aqueous solution: a kinetic study, React. Funct. Polym. 70 (2010) 707–714.
[39] Y. Zhang, F. He, S. Xia, L. Kong, D. Xu, Z. Wu, Adsorption of sediment phosphorus by porous ceramic filter media coated with nano-titanium dioxide film, Ecol. Eng. 64 (2014) 186–192.
[40] G. Li, S. Gao, G. Zhang, X. Zhang, Enhanced adsorption of phosphate from aqueous solution by nanostructured iron(III)-copper(II) binary oxides, Chem. Eng. J. 235 (2014) 124–131.
[41] X. Zheng, J. Pan, F. Zhang, E. Liu, W. Shi, Y. Yan, Fabrication of free-standing bio-template mesoporous hybrid film for high and selective phosphate removal, Chem. Eng. J. 284 (2016) 879–887.
[42] B. Kiran, A. Kaushik, Chromium binding capacity of *Lyngbya putealis* exopolysaccharides, Biochem. Eng. J. 38 (2008) 47–54.
[43] X. Hu, J. Wang, Y. Liu, X. Li, G. Zeng, Z. Bao, X. Zeng, A. Chen, F. Long, Adsorption of chromium (VI) by ethylenediamine-modified cross-linked magnetic chitosan resin: isotherms, kinetics and thermodynamics, J. Hazard. Mater. 185 (2011) 306–314.
[44] Y. Hu, T. Guo, X. Ye, Q. Li, M. Guo, H. Liu, Z. Wu, Dye adsorption by resins: Effect of ionic strength on hydrophobic and electrostatic interactions, Chem. Eng. J. 228 (2013) 392–397.
[45] L. Lai, Q. Xie, L. Chi, W. Gu, D. Wu, Adsorption of phosphate from water by easily separable Fe_3O_4@SiO_2 core/shell magnetic nanoparticles functionalized with hydrous lanthanum oxide, J. Colloid Interface Sci. 465 (2016) 76–82.
[46] L. Bai, C. Wang, L. He, Y. Pei, Influence of the inherent properties of drinking water treatment residuals on their phosphorus adsorption capacities, J. Environ. Sci. (China) 26 (2014) 2397–2405.
[47] W. Huang, X. Yu, J. Tang, Y. Zhu, Y. Zhang, D. Li, Enhanced adsorption of phosphate by flower-like mesoporous silica spheres loaded with lanthanum, Microporous Mesoporous Mater. 217 (2015) 225–232.
[48] J. Stejskal, J. Prokeš, M. Trchová, Reprotonated polyanilines: the stability of conductivity at elevated temperature, Polym. Degrad. Stab. 102 (2014) 67–73.
[49] J. Chen, J. Feng, W. Yan, Facile synthesis of a polythiophene/TiO_2 particle composite in aqueous medium and its adsorption performance for Pb(II), RSC Adv. 5 (2015) 86945–86953.
[50] N. Wang, J. Li, W. Lv, J. Feng, W. Yan, Synthesis of polyaniline/TiO_2 composite with excellent adsorption performance on acid red G, RSC Adv. 5 (2015) 21132–21141.
[51] Y. Zhang, B. Pan, C. Shan, X. Gao, Enhanced phosphate removal by nanosized hydrated La(III) oxide confined in cross-linked polystyrene networks, Environ. Sci. Technol. 50 (2016) 1447–1454.
[52] T. Sugimoto, X. Zhou, A. Muramatsu, Synthesis of uniform anatase TiO_2 nanoparticles by gel–sol method, J. Colloid Interface Sci. 259 (2003) 43–52.
[53] T. Sugimoto, X. Zhou, Synthesis of uniform anatase TiO_2 nanoparticles by the gel-sol method 2. Adsorption of OH^- Ions to $Ti(OH)_4$ gel and TiO_2 particles, J. Colloid Interface Sci. 252 (2002) 347–353.
[54] G. Ćirić-Marjanović, Recent advances in polyaniline research: polymerization mechanisms, structural aspects, properties and applications, Synth. Met. 177 (2013) 1–47.